

The single-electron transport in a three-ion magnetic molecule modulated by a transverse field

Javier I. Romero* and Eduardo R. Mucciolo†

Department of Physics, University of Central Florida, Orlando, Florida 32816, USA

(Dated: May 25, 2022)

We study single-electron transport in a three-ion molecule with strong uniaxial anisotropy and in the presence of a transverse magnetic field. Two magnetic ions are connected to each other through a third, nonmagnetic ion. The magnetic ions are coupled to ideal metallic leads and a back gate voltage is applied to the molecule, forming a field-effect transistor. The microscopic Hamiltonian describing this system includes inter-ion hopping, on-site repulsions, and magnetic anisotropies. For a range of values of the parameters of the Hamiltonian, we obtain an energy spectrum similar to that of single-molecule magnets in the giant-spin approximation where the two states with maximum spin projection along the uniaxial anisotropy axis are well separated from other states. In addition, upon applying an external in-plane magnetic field, the energy gap between the ground and first excited states of the molecule oscillates, going to zero at certain special values of the field, in analogy to the diabolical points resulting from Berry phase interference in the giant spin model. Thus, our microscopic model provides the same phenomenological behavior expected from the giant spin model of a single-molecule magnet but with direct access to the internal structure of the molecule, thus making it more appropriate for realistic electronic transport studies. To illustrate this point, the nonlinear electronic transport in the sequential tunneling regime is evaluated for values of the field near these degeneracy points. We show that the existence of these points has a clear signature in the $I - V$ characteristics of the molecule, most notably the modulation of excitation lines in the differential conductance.

I. INTRODUCTION

From the various types of magnetic states in matter, ferromagnetism and its microscopic causes is one of the most intriguing topics. A very singular class of magnetic systems are single-molecule magnets (SMMs).¹⁻³ Molecules in this class typically have a large net spin ground state and exhibit unusual attributes such as quantum tunneling of the magnetization (QTM),^{4,5} a relatively large decoherence time,⁶ and Berry-phase interference effects in the presence of magnetic fields.^{7,8} Commonly, SMMs are composed of transition metal ions (open $3d$ or $4f$ shells) bridged by ligand atoms and molecules. The phenomenological Hamiltonian that describes the magnetic properties of SMMs is the so-called giant spin approximation (GSA) model. For instance, in its simplest form, the GSA Hamiltonian can be written as

$$H_{\text{GSA}} = -D S_z^2 + E (S_x^2 - S_y^2), \quad (1)$$

The net magnetization has a preferential direction (an easy axis z in this example) as a consequence of the dominant uniaxial anisotropy ($D \ll E$). The in-plane transverse anisotropy allows the total spin to transit between different values of S_z . In this particular example, the molecule has a predominant second-order anisotropy signaling a rhombic symmetry.

A more microscopic description of SMMs comes from considering interactions at the ion level. In this case, one uses instead a multi-spin Hamiltonian of the type

$$H_{\text{ms}} = \sum_i [-d_i S_{iz}^2 + e_i (S_{ix}^2 - S_{iy}^2)] - \sum_{i \neq j} J_{ij} \vec{S}_i \cdot \vec{S}_j. \quad (2)$$

Here each magnetic site of the molecule has local uniaxial and transverse anisotropies d_i and e_i , respectively. In addition, there is an effective isotropic ferromagnetic interaction between pairs of sites parametrized by $J_{ij} > 0$, which contributes to the energy splitting of states with different total spin. (Some molecules are better described by an anisotropic J_{ij} .) We note that the on-site anisotropy terms (proportional to d_i and e_i) in Eq. (2) are meaningful only when the total spin of each site is $S_i \geq 1$.

The accuracy of the GSA and the multi-spin models was investigated in Ref. 9 by studying the connection between molecular and single-ion uniaxial anisotropies. Anisotropies in SMMs are very sensitive to the orientation of the ligands with respect to each magnetic ion, thus the energy spectrum of SMMs varies greatly with magnetic site symmetries. For instance, in the case of zero transverse anisotropies ($e_i = 0$ and, consequently, $E = 0$), the Hamiltonians in Eqs. (1) and (2) yield a two-fold degenerate ground state involving spin states parallel ($S_z = S$) and anti-parallel ($S_z = -S$) to the uniaxial anisotropy axis. If the transverse anisotropy terms (e_i and E) are nonzero, then the rotational S_z symmetry is broken and the two-fold degeneracy is lifted, with the ground and first excited states now being anti-symmetric and symmetric combinations of the $S_z = \pm S$ states. In general, the parameters used in the multi-spin approach depend on the intra-site or inter-site interactions between orbitals of the ligands and transition metals, but due to the large Hilbert space involved and the strong interplay between the many microscopic parameters, it is very challenging to take into account explicitly the overlap between orbitals and their symmetries for large magnetic molecules. One often employs the em-

pirical Goodenough-Kanamori rules^{10,11} that dictate the nature of interaction between magnetic ions. In addition, one also includes an effective interaction intermediated by diamagnetic atoms (the Anderson superexchange interaction).¹²

In recent years, interest emerged in exploring how the magnetic properties of SMMs may affect the molecule's electronic transport properties. Effects due to the QTM,¹³ Berry-phase interference,^{14,15} and their interplay with the Kondo resonance^{16,17} have been proposed. Several authors have also used first-principles calculations to investigate the electronic configuration, the magnetic properties, and coherent transport in SMMs.^{18–21} In addition, many important contributions have been made in studying the sequential transport for different molecular setups,^{22,23} as well as sequential transport dependence on spin-orbit coupling, the Jahn-Teller effect, and ligand charge variations.^{24–26}

In this paper, we investigate the dependence of sequential tunneling transport on an transverse magnetic field applied to a three-ion model that contains the essential microscopic details necessary for reproducing a SMM behavior. The microscopic model comprises two magnetic ions bridged by a third diamagnetic ion and takes into account the valence, ligand fields, and orbital energies of the ions, as well as direct and exchange Coulomb interactions present in the molecule. Our goal is to develop a simple phenomenological microscopic model of a SMM that goes beyond the giant spin Hamiltonian model and is amenable to realistic electronic transport studies.

We explore the energy spectrum of this system for several points in the parameter space of the Hamiltonian. We find that for a certain parameter range a magnetic bistability, similar to that observed for SMMs, develops. This bistability is characterized by a ground state degeneracy point and is driven by a magnetic field perpendicular to the molecule's main anisotropy axis. The modulation of the transition between magnetic states through a transverse magnetic field is one of the most unusual features of SMMs and is fully reproduced by our model. In the context of the giant spin model of an SMM, this modulation is understood as the result of Berry-phase interference of multiple spin tunneling paths, which in turn lead to the appearance of diabolical points in the molecule's spectrum.²⁷ In contrast, Our model contains many degrees of freedom and there are no easily identified topological phases. Instead, the modulation in our model arises from changes in electronic correlations when a finite transverse field is present. We evaluate the incoherent electronic transport through the molecule near this bistability. At the degeneracy points, states with opposite spins are decoupled, resulting in a clear qualitative change in the differential conductance of the molecule.

The paper is organized as follows: In Sec. II we describe the model Hamiltonian for the three-ion magnetic molecule. In Sec. III we present our choice of model parameters and the energy spectrum and symmetry of the states of the molecule. In Sec. IV we evaluate the sequen-

tial current and differential conductance of the molecule for in-plane magnetic fields ranging between zero and the nearest degeneracy point. In Sec. V we discuss the effects of spin tunneling modulation by a magnetic field on transport. Finally, in Sec. VI, we analyze our results and draw some conclusions.

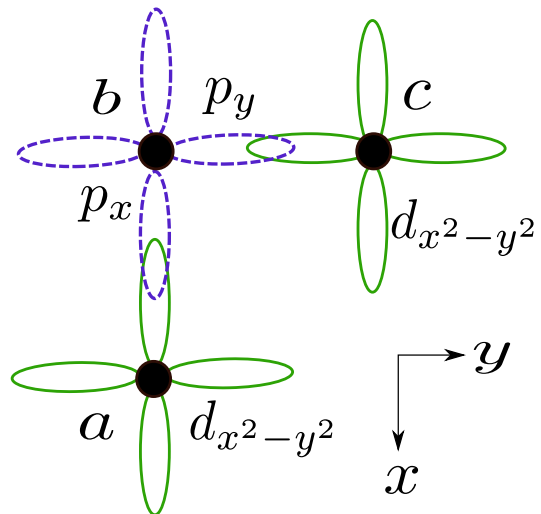


Figure 1: (Color online) Scheme of a simple three-ion SMM. For simplicity, we do not depict the rhombic ligand environment surrounding ions a and c . The magnetic ions labeled a and c interact through the diamagnetic ligand ion b with a bond angle of $\theta = \pi/2$, so that the $d_{x^2-y^2}$ orbitals (green/solid lobes) overlap with the p_x and p_y orbitals (purple/dashed lobes) of the ligand separately.

II. THE THREE-ION MODEL OF A SMM

A minimal realistic molecular core capable of reproducing the main features of a SMM such as large total spin ($S > 1/2$), uniaxial and in-plane anisotropies, and transverse field modulation consists of two transition metal ions bridged by a diamagnetic ligand ion. Consider the system shown schematically in Fig. 1. The two transition metal ions a and c have a $3d^8$ electronic configuration and a total spin $S = 1$ each. They interact magnetically through a superexchange interaction intermediated by a diamagnetic O^{2-} ion (electronic configuration $2p^6$), represented by b in Fig. 1. The five-fold degeneracy of the $3d$ orbitals in the magnetic ions is broken due to the bonding to ligands. To simulate such an effect, we assume that a weak orthorhombic ligand field acts on a and c , inducing local uniaxial and transverse anisotropies on each site. Thus, for an orthorhombic symmetry (D_{2h} point group), the ground states of ions a and c have two occupied unpaired single-particle orbitals ($a_{1,2}$ and $c_{1,2}$, respectively) which are symmetric and antisymmetric combinations of $d_{x^2-y^2}$ and $d_{3z^2-r^2}$ d states. We also consider a 90° angle between their bonds. As a result, the $d_{x^2-y^2}$ components of the single-particle

orbitals in both ions a and c overlap separately with the $p_{x,y}$ orbitals $b_{1,2}$ of ion b . Under this assumption, we use the appropriate Slater-Koster two-center integrals, which then yields $E_{p_x, d_{x^2-y^2}} = E_{p_y, d_{x^2-y^2}} = (pd\sigma)\sqrt{3}/2$. This configuration favors a ferromagnetic superexchange interaction. In our case the $E_{p_z, d_{3z^2-r^2}}$ and $E_{p_x, y, d_{x^2-y^2}}$ two-center integrals are zero.

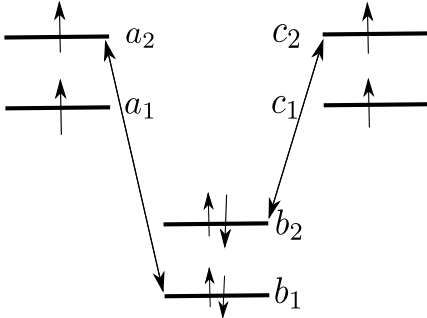


Figure 2: Scheme of the electron hopping (double-arrow lines) between magnetic ions and the diamagnetic ion. For a $3d^8$ ion in a weak orthorhombic ligand field (i.e., with a small distortion to rhombic symmetry), the unpaired single-particle orbitals (say for ion a) are $\psi_{a_2} = \kappa_1 d_{x^2-y^2} + \kappa_2 d_{3z^2-r^2}$ and $\psi_{a_1} = \kappa_1 d_{3z^2-r^2} - \kappa_2 d_{x^2-y^2}$, where $\kappa_1^2 + \kappa_2^2 = 1$. Since the rhombic contribution to the ligand field is small, we regard the mixing amplitude κ_2 between the initially degenerate unpaired orbitals as a small parameter: $|\kappa_2| \ll |\kappa_1|$.

The scheme of these selective orbital overlaps is shown in Fig. 2. The features of our model are captured by the effective Hamiltonian

$$H_{\text{mol}} = H_a + H_b + H_c + H_{ab} + H_{bc}, \quad (3)$$

where H_α , with $\alpha = a, c$ denotes the Hamiltonian for a magnetic ion,

$$\begin{aligned} H_\alpha = & \sum_{i=1,2} \varepsilon_{M,i} n_{\alpha_i,\sigma} + U_M \sum_{i=1,2} \sum_{\sigma=\uparrow,\downarrow} n_{\alpha_i,\uparrow} n_{\alpha_i,\downarrow} \\ & + U'_M \sum_{\sigma,\sigma'=\uparrow,\downarrow} n_{\alpha_1,\sigma} n_{\alpha_2,\sigma'} - J_M \vec{S}_{\alpha_1} \cdot \vec{S}_{\alpha_2} \\ & - d S_{z,\alpha}^2 + e (S_{x,\alpha}^2 - S_{y,\alpha}^2), \end{aligned} \quad (4)$$

and H_b describes the diamagnetic ion,

$$\begin{aligned} H_b = & \varepsilon_O \sum_{i=1,2} n_{b_i,\sigma} + U_O \sum_{i=1,2} \sum_{\sigma=\uparrow,\downarrow} n_{b_i,\uparrow} n_{b_i,\downarrow} \\ & + U'_O \sum_{\sigma,\sigma'=\uparrow,\downarrow} n_{b_1,\sigma} n_{b_2,\sigma'} - J_O \vec{S}_{b_1} \cdot \vec{S}_{b_2}. \end{aligned} \quad (5)$$

For simplicity we consider that the a and c ions have identical rhombic symmetries and therefore they have the same interaction strengths, orbital energies, and anisotropy parameters. We allow for a crystal field splitting of the magnetic ion orbitals, but assume that the orbitals in the diamagnetic ion are degenerate. In Eq.

(3), H_{ab} and H_{bc} describe electron hopping between the magnetic ions and the diamagnetic ion,

$$H_{ab} = t \sum_{\sigma=\uparrow,\downarrow} (c_{a_2,\sigma}^\dagger c_{b_1,\sigma} + \text{H.c.}) \quad (6)$$

and

$$H_{bc} = t \sum_{\sigma=\uparrow,\downarrow} (c_{b_2,\sigma}^\dagger c_{c_2,\sigma} + \text{H.c.}), \quad (7)$$

with $\alpha = a, c$. In Eqs. (4), (6), and (7), $n_{\alpha_i,\sigma} = c_{\alpha_i,\sigma}^\dagger c_{\alpha_i,\sigma}$, where $c_{\alpha_i,\sigma}^\dagger$ ($c_{\alpha_i,\sigma}$) creates (annihilates) an electron with z spin projection σ in the orbital i of ion $\alpha = a, b, c$ and satisfy the standard fermionic anticommutation relations. The total spin operator associated to an orbital i in ion α is \vec{S}_{α_i} while $\vec{S}_\alpha = \vec{S}_{\alpha_1} + \vec{S}_{\alpha_2}$.

The first term on the r.h.s of Eqs. (4) and (4) accounts for the single-particle orbital energies, while the second and third terms represent the on-site and intra-site Coulomb repulsion within ion α . The fourth term enforces Hund's first rule, maximizing the total spin on each ion ($J_\alpha > 0$). The last two terms on the r.h.s. of Eq. (4) are the uniaxial and transverse on-site anisotropies produced by the rhombic ligand field environment and by the spin-orbit coupling within each magnetic ion.

III. ADJUSTING THE MODEL PARAMETERS

The model Hamiltonian in Eq. (3) has a large number of parameters that have to be properly adjusted in order to produce the phenomenology expected of a SMM. Below, we discuss our choices of parameter values. We first consider the Hamiltonian in the absence of transverse anisotropies ($e_\alpha = 0$). Then we include non-zero e_α terms, and an in-plane external magnetic field in order to produce degeneracy points in the spectrum of the molecule.

A. Total S_z spin in the absence of transverse anisotropy

The lowest energy states of a SMM typically have a large total spin S , with the maximum spin projection $|S_z| = S$ happening at the ground state, followed by excited states corresponding to decreasing spin projections. A convenient way to produce such a spectrum in our model is to start with S_z as a good quantum number by setting $e_\alpha = 0$. Then, for different choices of the parameters $\varepsilon_{M,i}$, ε_O , U_M , U'_M , U_O , U'_O , J_M , J_O and d , we calculate the total S_z spin of the molecule as a function of t . For the states with maximum possible spin, $S = 2$ for our three-ion model, we compare their composition to that expected for a state obtained by adding two $S = 1$ spin states. Even though U'_M and U'_O are nonzero in a real molecule, we have found that they have little qualitative importance in our results. Thus, for the sake of

simplicity and in order to decrease our parameter space, we have set them equal to zero.

Realistic values for some parameters can be obtained from the review by Imada, Fujimori, and Tokura²⁸ and the recent work by Kim and Min²⁹ using NiO systems as a reference. Thus, from the data in Table III of Ref. 28 we set the on-site Coulomb repulsion between d electrons to $U_M = 7$ eV. Typical values for the on-site Coulomb repulsion of p-electrons are in the range from 4 – 7 eV (see Refs. 30 and 31). Here, we assume $U_O = 4$ eV. From table III of Ref. 28, the Hund's rule parameter for the magnetic ion is set to $J_M = 0.95$ eV. For the diamagnetic ion, we choose a slightly larger value, $J_O = 1.5$ eV in order to yield a spectrum similar to that of a ferromagnetic SMM. The orbital energies in the magnetic ions are obtained from Fig. 59 of Ref. 28: $\epsilon_1^M - \epsilon_O = 0.66$ eV and $\epsilon_2^M - \epsilon_O = 0.72$ eV. For convenience, we shift the total energy such that $\epsilon_O = 0$. The energy splitting between the two orbitals of the magnetic ions, $\epsilon_2^M - \epsilon_1^O = \Delta\epsilon_{\text{crystal}}$ is due to the crystal field splitting produced by the surrounding ligands. In Ref. 32, rhombic crystal field parameters are found to be of the order of meV or smaller; we choose the splitting to be about 10 meV.

Based on the EPR measurements in Ref. 9, the uniaxial anisotropy parameter is set to $d = 0.6$ meV (equivalent to 7 K). Figure 3 shows $|S_z|$ for the ground state (two-fold degenerate), first excited state (two-fold degenerate), and second excited state (nondegenerate) versus the hopping parameter t . It is clear that for the parameter we chose, the ground state has the highest possible total spin, $S = 2$. For $t > 0.75$ eV, states with total spin projection $|S_z| = 1$ become the first excited states, while the state with total spin projection zero moves up to the second excited state position. This is the typical case for a SMM within the description provided by the GSA Hamiltonian of Eq. (1).

B. Anisotropy and degeneracy points

We now consider the inclusion of local transverse anisotropies that make the eigenstates of the Hamiltonian to be symmetric and antisymmetric combinations of $|S_z\rangle$ states. In addition, we consider the effect of an applied transverse (in-plane) magnetic field on the molecule's energy spectrum. The transverse field Hamiltonian is given by

$$H_{\text{field}} = b \left(\sum_{\alpha=a,c} g_{x,\alpha} S_{x,\alpha} \cos \phi + g_{y,\alpha} S_{y,\alpha} \sin \phi \right), \quad (8)$$

where $b = \mu_B |\vec{B}|$ and $\vec{B} = (B \cos \phi, B \sin \phi, 0)$ is the external magnetic field. Following Refs. 33 and 34, a reasonable estimate of the anisotropic g -factors would be $g_{x,\alpha} = 2.270$ and $g_{y,\alpha} = 2.269$. We set the hopping amplitude to $t = 0.8$ eV, while the transverse anisotropy parameter is set to $e = 5 \mu\text{eV}$, which is less than 1% of the uniaxial anisotropy parameter d . We do not consider

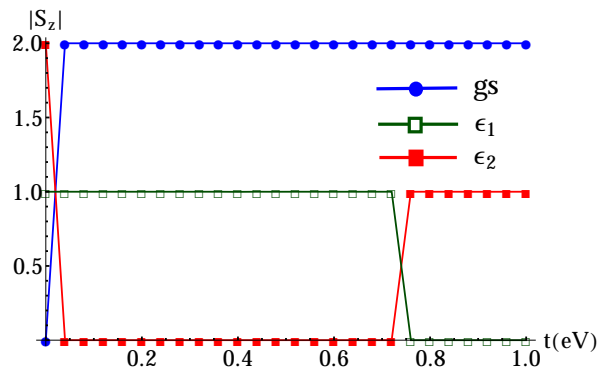


Figure 3: (Color online) Total spin projection S_z of the molecule. For $0 < t < 1.2$ eV, the lowest energy level is a $|\pm 2\rangle$ state, the first excited state has $S_z = 0$, while the next (degenerate) excited states have $S_z = \pm 1$. We find the typical SMM behavior in the $0.7 \text{ eV} < t < 1$ eV range, where the first excited states have $S_z = \pm 1$ and the highest energy level has $S_z = 0$. The crossing in the graph denotes the point where total S_z spin changes for the first and second excited eigenstates. For $t = 0.77$ eV, the energy splitting between the two lowest eigenstates ($S_z = \pm 2$ and $S_z = \pm 1$) is of the order of the uniaxial anisotropy parameters d_α , with the value of $\Delta = 0.07 \text{ eV}$, while the splitting between $S_z = \pm 1$ and $S_z = 0$ is $\Delta = 0.5$ meV.

coupling of the magnetic field to the middle ion since it would change the energy levels of the high energy sector by a very small amount, given that $b \ll U$. The goal is to find ϕ and b such that the in-plane anisotropy brought by the external magnetic field compensates the intrinsic in-plane anisotropy of the magnetic ions, removing the splitting between states with maximum projection $|S_z|$, thus restoring degeneracy to the ground state.

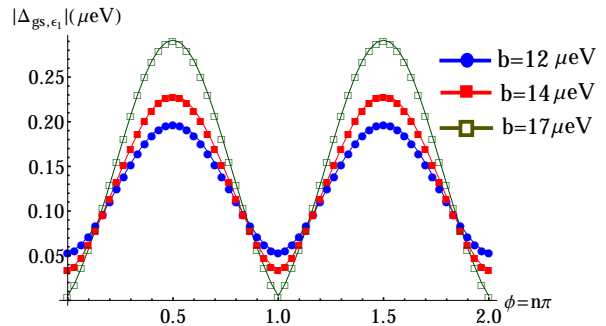


Figure 4: (Color online) Splitting of the two lowest energy levels versus the transverse field angle ϕ . The angle is measured with respect to the positive x axis. We see that for various values of the magnetic field, the lowest splitting occurs at $\phi = \pi$.

In Fig. 4, we show the resulting splitting of the two lowest energy levels versus the angle ϕ . The angle $\phi = \pi$ creates symmetric spin paths for the tunneling of the molecule's magnetization, leading to maximum destructive interference. In Fig. 5 the splitting is shown as a

function of the applied field magnitude b at this particular field direction ($\phi = \pi$). We observe that the second degeneracy point occurs approximately at twice the value of the first one. We note that the periodic modulation of the splitting with b is as characteristic feature of SMMs (see Refs. 4,7,27).

We now consider how the symmetry of the eigenstates is affected by changes in the magnitude of the magnetic field. For this purpose, we define the symmetry coefficient

$$C_\Sigma = \frac{1}{2}|C_1 + C_2|, \quad (9)$$

where $C_{1,2}$ are the amplitudes of the two degenerate states along the $S_z = \pm 2$ basis states. If $C_\Sigma = 0$ the eigenstate is antisymmetric, whereas if $C_\Sigma = C_{1,2}$ the eigenstate is symmetric. The results are presented in Fig. 6. We observe that the ground state changes from symmetric to antisymmetric at the first degeneracy point (left dashed line), while the first excited state does the reverse. The energy splitting between the linear combination of S_z states (symmetric and antisymmetric) vanishes at the degeneracy points.

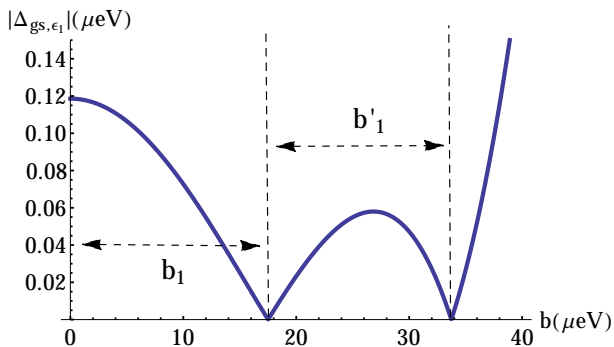


Figure 5: (Color online) Splitting of the two lowest energy levels versus the magnitude of the magnetic field b at an angle of $\phi = \pi$. We observe two degeneracy points where the splitting between the two lowest energy levels goes to zero. The first point occurs at $b \approx 18 \mu\text{eV}$ ($B \approx 0.3$ tesla), while the second one occurs at $b \approx 34 \mu\text{eV}$ ($B \approx 0.6$ tesla).

IV. SEQUENTIAL TRANSPORT THROUGH THE MOLECULE

While a fully-coherent transport approach can be used, it is not essential in describing theoretically the effect of the transverse magnetic field modulation on the SET I-V characteristics, which can be fully captured by a rate equation approach in the dc limit.

We study electronic transport in our model system by connecting the molecule to two reservoirs of noninteracting electrons. The current through the molecule can be controlled by applying a voltage difference between the reservoirs, as well as by changing the total charge

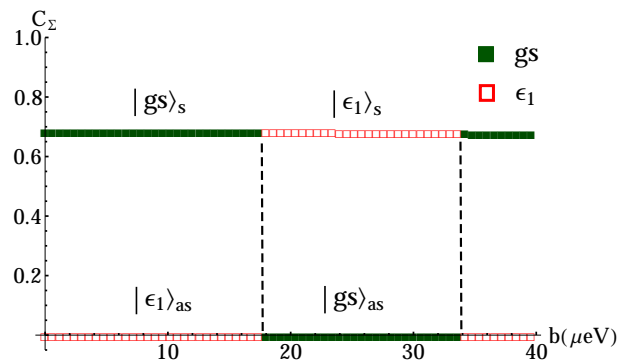


Figure 6: (Color online) Symmetry of the ground state (filled squares) and first excited state (empty squares) versus the magnetic field magnitude b . At $b = 0$ the ground and first excited states are $|\text{gs}\rangle = -0.68(|+2\rangle + |-2\rangle) + 0.27 \times (\text{contam.})$ and $|\epsilon_1\rangle = 0.69(|+2\rangle - |-2\rangle) + 0.22 \times (\text{contam.})$, respectively, where (contam.) represents a contribution from spin states other than $|\pm 2\rangle$. As the transverse magnetic field grows, the amplitude C_Σ tends to decrease, allowing for an increasing admixture with $S_z = 0$ states. At the second degeneracy point (right dashed line), the symmetry of the states changes again.

of the molecule through an applied back-gate voltage. We define a general charge-spin state by (n, S) where n and S denote the excess charge and the total spin of the molecule, respectively. For simplicity, we only consider transitions between two charge states ($n = 0, 1$). Initially, the molecule is in the state $(0, 2)$ where it has a $3d^8 - 2p^6 - 3d^8$ electronic configuration. We then allow one electron to hop from the reservoirs into the molecule and restrict it to be localized either on the a_1 or c_1 orbitals, bringing the molecule to the $(1, \frac{3}{2})$ state, which comprises both $3d^9 - 2p^6 - 3d^8$ and $3d^8 - 2p^6 - 3d^9$ electronic configurations.

We assume that the coupling to the reservoirs is such that there is equal probability for an electron to land in either one of the two magnetic ions. Since one of the ions changes its oxidation state when an electron is added, its anisotropy terms and the g -factors change as well (see Refs. 13, 16, 35, 36, and 37).

Concerning model parameters, we assume a *reduction* in the local uniaxial anisotropy of the ion upon changing its charge state and set $d'_\alpha = 0.3$ meV. It is worth noting that in the context of the GSA, the anisotropy parameters change their values upon varying the charge state of the molecule (see Ref. 40). In our transport analysis, d'_α does not play an essential role since we will focus on the contributions coming from the two lowest spin states of the $(1, 3/2)$ charge-spin sector which can only have pure (or combinations of) $S_z = \frac{3}{2}$ z -spin components. The modified transverse anisotropy e'_α does not take part in the Hamiltonian for the $(1, \frac{3}{2})$ configuration since the total spin of the ion receiving an electron becomes $S_\alpha = \frac{1}{2}$, turning the local ground state of the ion a Kramers doublet. Finally, for the sake of simplicity, we assume that

the same g factors used for the (0, 2) configuration.

In order to evaluate single-electron transport, we start by diagonalizing the Hamiltonian for different charge-spin configurations. We then solve a set of coupled differential equations for the time evolution of the quantum state probabilities of the molecule. This approach is suitable for describing incoherent, sequential transport across the molecule. In the context of our model, its use is justifiable because the phase of the itinerant electron does not play an essential role in the existence of degeneracy points in the molecule's spectrum. In other words, the situation is similar to that of a quantum dot where external parameters such as plunger gate voltages can tune the states available to an itinerant electrons tunneling in and out of the system regardless of the electron's phase coherence. The only necessary assumption for the rate equation approach to be valid is that the molecule should be weakly coupled to the leads and the temperature sufficiently low. These conditions can be cast as $\gamma, k_B T \ll |\Delta|$ (see notation below).

The rate equation describing the time evolution of the probability of the molecule to be in an arbitrary state m is given by³⁸

$$\frac{dp_m}{dt} = -p_m \sum_{m'} \Gamma_{m \rightarrow m'} + \sum_{m'} p_{m'} \Gamma_{m' \rightarrow m}, \quad (10)$$

where $\Gamma_{m \rightarrow m'}$ is the transition rate between different eigenstates m and m' . The first term on the r.h.s of Eq.(10) comprises outgoing terms describing the transition from an initial state m to a final state m' by either taking away or adding an extra electron. The second term represents processes where a final state m' transitions back to an initial state m (again, by means of either taking away or adding an extra electron). Equation (10) can be written in matrix form as

$$\frac{d\mathbf{P}}{dt} = \mathbf{\Gamma} \cdot \mathbf{P}, \quad (11)$$

where \mathbf{P} is a vector containing the probabilities $\{p_m\}$ and $\mathbf{\Gamma}$ is a matrix with entries $\{\Gamma_{mm'}\}$ which are related to the transition rates in the following way:

$$\begin{aligned} \Gamma_{mm'} &= \Gamma_{m' \rightarrow m} & \text{if } m \neq m' \\ \Gamma_{mm} &= - \sum_{m' \neq m} \Gamma_{m \rightarrow m'}. \end{aligned} \quad (12)$$

In the stationary regime, we look for the steady-state probabilities p_m such that $dp_m/dt = 0$. In matrix form, this is achieved by finding the eigenvector \mathbf{P} of the matrix $\mathbf{\Gamma}$ with a zero eigenvalue. The transition rates from a state m to a state m' when adding (or subtracting) electrons (e^-) to (from) the molecule are given by

$$\Gamma_{m \rightarrow m'}^\tau = \begin{cases} \gamma_{m',m}^\tau f_\tau(\mu_{m'm} - eV_\tau), & e^- \text{ in,} \\ \gamma_{m,m'}^\tau [1 - f_\tau(\mu_{mm'} - eV_\tau)], & e^- \text{ out} \end{cases} \quad (13)$$

where the index $\tau = L, R$ refers to the left and right reservoirs, respectively. Here, $f_\tau(x) = 1/(1 + e^{x/k_B T})$ is

the Fermi distribution of the left (L) or right (R) reservoirs. The electrochemical potential of the molecule, i.e., the energy required to go from a state m to state a m' , is defined as

$$\mu_{mm'} = \epsilon_m - \epsilon_{m'} - e\eta V_g, \quad (14)$$

where ϵ_m and $\epsilon_{m'}$ are the energy eigenvalues corresponding to eigenstates m and m' , respectively, and V_g is the backgate voltage (we set the lever arm coefficient $\eta = 1$). The coefficients $\gamma_{\beta,\beta'}^\tau$ are the tunneling rates between two eigenstates β and β' of the molecule and are given in the Golden rule approximation by

$$\gamma_{\beta,\beta'}^\tau = 2\pi\rho \sum_\sigma |T_{\beta\beta'}^{\sigma,\tau}|^2 \quad (15)$$

where ρ is the density of states of both reservoirs (here considered constant) and

$$T_{\beta\beta'}^{\sigma,\tau} = \sum_j t_{j,\tau} \langle \beta | c_{j\sigma}^\dagger | \beta' \rangle \quad (16)$$

denote the tunneling matrix elements. The operator $c_{\alpha j \sigma}^\dagger$ creates an electron with spin σ on the single-particle orbital j of ion α . To simplify the calculations we assume that $t_{j,\tau}$ is independent of the orbital, thus we drop the j index, also we assume that $t_L = t_R$. Since different charge configurations of the molecule involve states with different spin quantum numbers, selection rules for spin transitions become important in the transport calculations. The tunneling matrix elements satisfy the selection rules $|S_m - S_{m'}| = 1/2$, $|S_{zm} - S_{zm'}| = 1/2$ and $|N_m - N_{m'}| = 1$, for any two eigenstates of the Hamiltonian belonging to different charge-spin sectors. The net steady-state current through the left lead (we omit the L subscript) is given by

$$I = |e| \sum_{mm'} \Gamma_{m \rightarrow m'}^L p_m, \quad (17)$$

where m, m' are indexes for different charge states. In Eq. (17), multiply the r.h.s it by -1 if an electron is going out of the molecule and into the left reservoir.

V. EFFECT OF SPIN TUNNELING MODULATION ON TRANSPORT

Transport is evaluated for different values of the field between in the range $[0 : b_2]$, where b_S denotes the magnitude of the field for which a degeneracy point occurs for the charge-spin sector with total spin $S = 2$. In order to see signatures of magnetization tunneling interference on transport, we only consider transitions between the two lowest energy levels of each charge-spin sector, as shown in Fig. 7. The ground and first excited eigenstates of charge sector n are labeled as $|\text{gs}^{(n)}\rangle$ and $|\epsilon_1^{(n)}\rangle$, respectively. In Fig. 7, we see that for $b = 0$ the eigenstates of the (0, 2) configuration are linear combinations

of $|S_z = \pm 2\rangle$ spin states, while the ground state of the $(1, \frac{3}{2})$ sector is two-fold degenerate with the $|S_z = \pm \frac{3}{2}\rangle$ spin states having the same energy. For $b = b_2$ the tunnel splitting of the $(0, 2)$ configuration goes to zero and the ground state becomes the two-fold degenerate $|S_z = \pm 2\rangle$ spin states. As for the $(1, \frac{3}{2})$ sector, an energy splitting (Δ_{b_2}) is induced by the magnetic field, with the eigenstates being now a linear combination of $|S_z = \pm \frac{3}{2}\rangle$ spin states. In both cases, the corresponding selection rules allow transitions between all eigenstates.

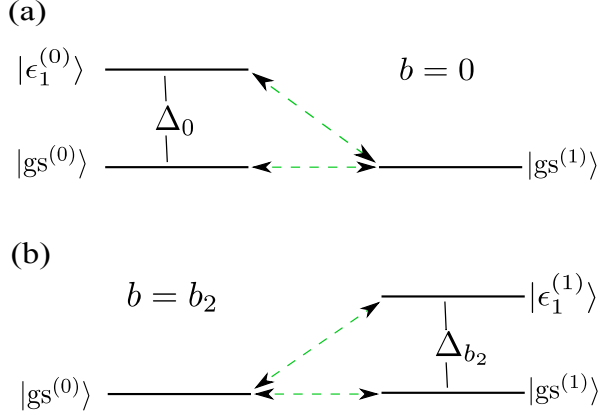


Figure 7: (Color online) Allowed transitions (dashed arrows) between the two lowest energy levels for the $(0, 2)$ and $(1, 3/2)$ charge-spin sectors. In (a), Δ_0 is the splitting between eigenstates for zero field ($b = 0$) while in (b) Δ_{b_2} is the splitting when the field is tuned to the degeneracy point ($b = b_2$).

Interesting physics can also be found if all combinations of S_z states corresponding to a particular total spin S of the molecule are considered. This is because anisotropy contributions tend to contaminate the lowest energy levels with a small admixture of $S_z = 0$ states, opening transitions in the transport that would otherwise have been forbidden by selection rules. A study of these contributions to transport within the GSA can be found in Ref. 16. Since we are primarily interested in how the modulation of the transverse anisotropy splitting affects transport, we only consider the two lowest energy S_z states. For other states, the energy cost to access different transitions would be too large compared to the energy gap generated by the transverse anisotropy.

We tune the gate voltage V_g so that the ground state energies for the $(0, 2)$ and $(1, \frac{3}{2})$ charge-spin sectors are aligned and vary V_g slightly around this point. Since the tunnel splitting due to transverse anisotropies is very small, of the order of the μeV (see Fig. 8), a very small temperature as well as a very low coupling $\gamma_{\beta, \beta'}^T$ are required to resolve features in the electronic transport that can be associated to the tunneling of the magnetization. Thus, we set the temperature in the reservoirs to $T = 0.1$ mK and choose the product $\rho |T_{\beta, \beta'}^T|^2$ so that both $k_B T$ and $\gamma_{\beta, \beta'}^T$ are much smaller than the energy level separation within the molecule. We note that while, in practice, a small value for $\gamma_{\beta, \beta'}^T$ can be achieved by chemi-

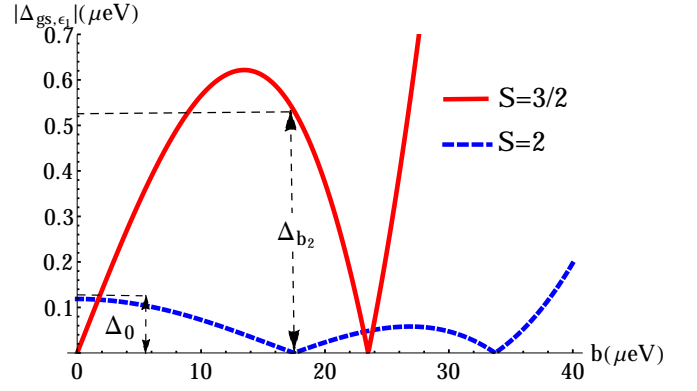


Figure 8: Splittings between the two lowest energy levels for the $S = 3/2$ (solid line) and $S = 2$ (dashed line) total spin sectors. The first degeneracy point for $S = 2$ is at $b_2 \approx 18 \mu\text{eV}$ (equivalent to 0.3 tesla).

cally engineering the SMM ligands, arriving at such low temperatures in single-electron transistor setups is quite challenging.

The left-lead current (I) to/from the molecule is shown in Fig. 9. For $b = 0$, transitions between excited and ground states are seen in the current steps at zero bias voltage and at $V_b/k_B T \approx \pm 13$. When $b = b_2$, these steps can be seen instead at $V_b/k_B T \approx \pm 61$. Figure 10 shows a plot of the differential conductance (dI/dV_b) as a function of the bias voltage and the magnetic field. Resonance peaks seen at $b' = 0$ and $b' = 1$ correspond to the current steps of Fig. 9. As one approaches the degeneracy point ($b' = 1$), the conductance peak corresponding to the $|gs^{(1)}\rangle \leftrightarrow |\epsilon_1^{(0)}\rangle$ transition is shifted towards the larger conductance peak (at $V_b' = 0$). At the degeneracy point, this peak is absorbed by the zero-bias conductance peak, increasing the current flow between the ground states of the molecule. In addition, we notice that the conductance decreases when the field is close to zero. We also observe that new resonances appear as a consequence of the field-induced energy gap of the $(1, \frac{3}{2})$ charge-spin sector. These can be seen in the conductance peaks coming out of the zero-bias and $|gs^{(1)}\rangle \leftrightarrow |\epsilon_1^{(0)}\rangle$ transition resonance peaks in the $b' = 0$ plane. For some values of the field, conductance peaks arise as resonances merge with each other. These peaks appear when the electrochemical potentials in the dot are the same i.e., $\mu_{gs^{(0)}, \epsilon_1^{(1)}} = \mu_{\epsilon_1^{(0)}, \epsilon_1^{(1)}}$, $\mu_{gs^{(0)}, gs^{(1)}} = \mu_{\epsilon_1^{(0)}, \epsilon_1^{(1)}}$, and $\mu_{gs^{(1)}, \epsilon_1^{(0)}} = \mu_{\epsilon_1^{(0)}, \epsilon_1^{(1)}}$. Figures 11 and 12 show contour plots of the differential conductance versus bias and gate voltage. The positive slope line seen for $b = 0$ in Fig. 11 corresponds to the $|gs^{(1)}\rangle \leftrightarrow |\epsilon_1^{(0)}\rangle$ transition and is eliminated upon tuning the field to the degeneracy point. At the same time, the applied magnetic field creates an energy gap allowing the $|gs^{(0)}\rangle \leftrightarrow |\epsilon_1^{(1)}\rangle$ transition, which corresponds to the negative slope line in Fig. 12.

In Figs. 11 and 12, in order to show in detail the fine features that appear upon crossing a degeneracy point,

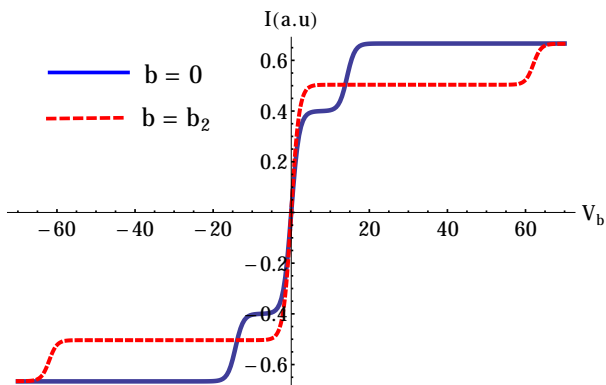


Figure 9: Current through left lead versus bias voltage at $b = 0$ (solid line) and $b = b_2$ (dashed line) for $T = 1$ mK (current is shown in arbitrary units). The bias voltage is plotted in units of $k_B T / |e|$. The gate voltage for each curve is such that the ground states for the two charge sectors involved are aligned.

the gate voltage V_g was shifted and rescaled: $V'_g = (V_g - V_s) \times 10^3$, where $eV_s = 8.169$ eV.

VI. CONCLUSION

We have studied the incoherent electronic transport through an anisotropic magnetic molecule using a microscopic model that provides spectral properties similar to

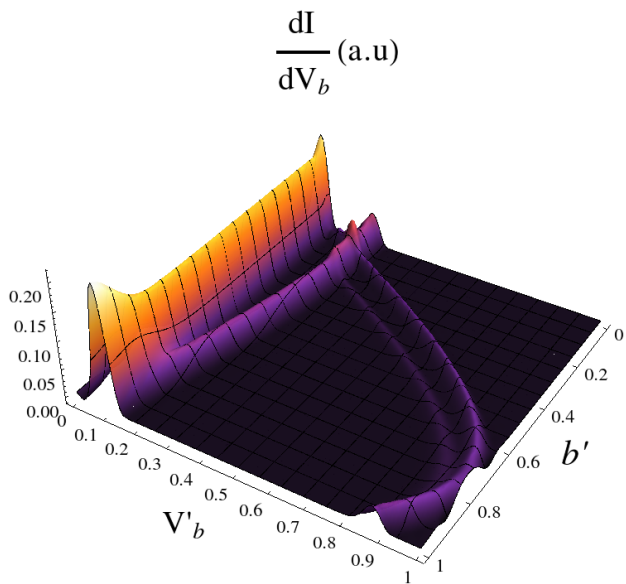


Figure 10: Plot of the differential conductance dI/dV_b as a function of the dimensionless bias voltage $V'_b = V_b/V_{\max}$ (here $V_{\max} = 75k_B T / |e|$) and the dimensionless magnetic field $b' = b/b_2$. The gate voltage is varied so that the ground states of the two charge sectors, $(0, 2)$ and $(1, \frac{3}{2})$, are kept aligned. The differential conductance is given in arbitrary units.

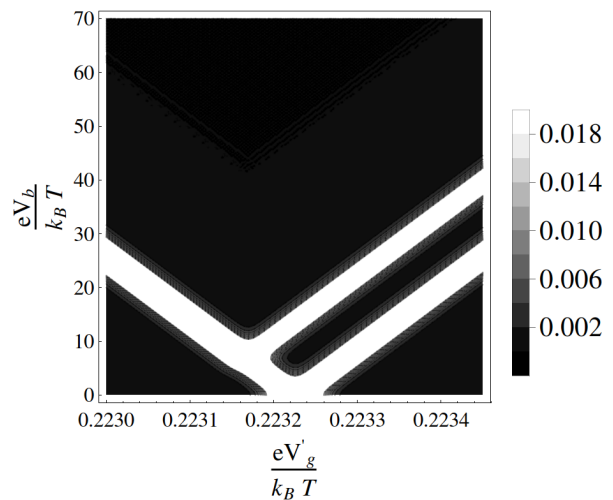


Figure 11: Contour plot of the differential conductance dI/dV_b as a function of bias and gate voltage at $b = 0$.

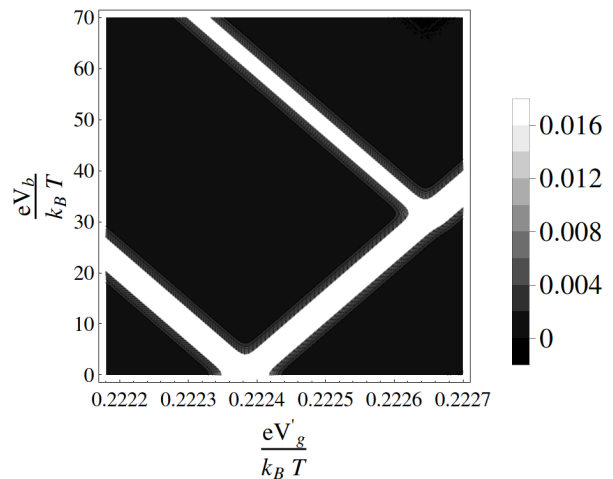


Figure 12: Contour plot of the differential conductance, dI/dV in arbitrary units, as a function of bias and gate voltage at $b = b_2$.

those of a multi-ion single-molecule magnet. By describing the molecule's core as a set of a few multi-orbital quantum dots, we open the door to a better understanding of the interplay between internal degrees of freedom of the molecule and its transport properties. This cannot be done within the giant spin approximation which is usually the starting point for characterizing the behavior of SMMs.

Another advantage of our model is its simplicity: by reducing the degrees of freedom to a manageable number, the model makes it possible to study in more detail the influence of the molecule's geometry and ion arrangement, as well as of the electron path across the molecule, on transport. In addition, by keeping the number of degrees of freedom small, it might be possible to go beyond the incoherent regime and use this model to study strongly

correlated phenomena such as the Kondo effect. These are currently out of the reach of fully atomistic calculations, such as those of Refs. 20 and 21.

Our model captures the essential phenomenology of a SMM, including the quantum tunneling of the net magnetization. We have illustrated this point by showing a modulation of the non-linear I-V characteristics upon the application of an transverse magnetic field. The appearance and disappearance of resonance lines is a clear indication of the existence of degeneracy points in the molecule's spectrum at certain values and directions of the transverse field. This behavior is similar to what is expected for a SMM in the giant spin approximation, where the destructive interference between tunneling trajectories of the giant spin create a periodic dependence on the transverse field. However, the lack of a well-defined topological phase in our model prevents us from making a direct connection between the modulation we observe and Berry phase interference.

Our model does have some limitations. For instance, we restrict the orbitals that participate in the hopping terms of the molecule's Hamiltonian. In addition, not all configurations are included and the interactions with ligands is only taken into account in at a phenomenological level.

The energy spectrum in our model is very sensitive to the choice of parameters and there is a complex interplay between the different interactions present in the model. In general, on-site anisotropies, Coulomb and overlap interactions intra and inter transition metals are not trivial to estimate. We have tried to use realistic or reasonable values whenever possible. These parameters depend on the electronic structure of the magnetic ions as well as on the geometrical configuration of the ligands surrounding the magnetic core. The bond angle between two magnetic ions is also of key importance in our calculations. For the particular three-ion model we studied, we chose a right bond angle to be 90 degrees and magnetic ions with parallel anisotropies. This allowed us to neglect the sigma overlap between the $d_{x^2-y^2}$ orbitals of the magnetic ions and the p_z orbital of the bridging diamagnetic ion, as well as to prevent any contamination by $d_{3z^2-r^2}$ orbitals. The result was an effective superexchange ferromagnetic interaction that competed with the $S_z = 0$ ground state favored by the local uniaxial anisotropies. Even with all

these constraints, we found that the model Hamiltonian yielded a high-spin, tunneling-split ground state, as it is typical for SMMs. A crucial parameter for our study is the on-site in-plane anisotropy e , which controls the splitting and competes with the in-plane magnetic field.

Our calculations show that at very low temperatures certain transitions are suppressed when a transverse magnetic field is tuned to a special direction and value that make the ground state twofold degenerate. This has a direct effect on non-equilibrium electronic transport across the molecule. At small enough bias voltages, the effect of the external field when tuned in-between the degeneracy points is to modulate the access to excited states. This in turn shifts the peaks in the dI/dV response in an amount proportionally to the tunnel splitting of spin states.

The fact that we have to rely on very low temperature (in the mili-Kelvin range) to visualize these features indicates that they will be challenging to observe experimentally. Molecules with a large tunnel splitting are better suited for exploring the interplay between transport and quantum tunneling of the magnetization. This will require a relatively strong in-plane anisotropy as compared to the uniaxial anisotropy, which goes somewhat against the usual synthesis effort, which aims at increasing the uniaxial anisotropy. It is worth noting that recent advances in experimental setups indicate that small splittings may be observable.^{39,40}

We plan to further explore our microscopic formulation to consider more complex molecules with multi-ion transition-metal cores. We are currently extending our approach to investigate field modulation effects in the electronic transport of mononuclear SMMs, which consist of one rare-earth ion within a ligand cage. These systems have been synthesized with success in recent years (see for instance Refs. 41–44).

Acknowledgments

This work was supported by NSF ECCS under Grant No. 1001755. The authors would like to thank Enrique del Barco, George Martins, and Edson Vernek for valuable comments.

* Electronic address: jromerobohorquez@knights.ucf.edu

† Electronic address: mucciolo@physics.ucf.edu

¹ G. Christou, D. Gatteschi, D. N. Hendrickson, and R. Sessoli, *MRS Bulletin* **25**, 66 (2000).

² D. Gatteschi, R. Sessoli, and J. Villain, *Molecular Nanomagnets* (Oxford University Press, New York, 2007).

³ J. Friedman and M. P. Sarachik, *Annu. Rev. Condens. Matter. Phys.* **1**, 109 (2010).

⁴ J. R. Friedman, M. P. Sarachik, J. Tejada, and R. Ziolo, *Phys. Rev. Lett.* **76**, 3830 (1996).

⁵ L. Thomas, F. Lioni, R. Ballou, D. Gatteschi, R. Sessoli, and B. Barbara, *Nature (London)* **383**, 145 (1996).

⁶ A. Ardavan *et al.*, *Phys. Rev. Lett.* **98**, 057201 (2007).

⁷ W. Wernsdorfer and R. Sessoli, *Science* **284**, 133 (1999).

⁸ H. M. Quddusi *et al.*, *Phys. Rev. Lett.* **106**, 227201 (2011).

⁹ S. Hill *et al.*, *Dalton Trans.* **39**, 4693 (2010).

¹⁰ J. B. Goodenough, *Phys. Rev.* **100**, 564 (1955).

¹¹ J. Kanamori, *J. Phys. Chem. Solids* **10**, 87 (1959).

¹² P. W. Anderson, *Phys. Rev.* **79**, 350 (1950).

¹³ C. Romeike, M. R. Wegewijs, W. Hofstetter, and H.

- Schoeller Phys. Rev. Lett. **96**, 196601 (2006).
- ¹⁴ G. Gonzalez and M. N. Leuenberger, Phys. Rev. Lett. **98**, 256804 (2007).
- ¹⁵ M. N. Leuenberger and E. R. Mucciolo, Phys. Rev. Lett. **97**, 126601 (2006).
- ¹⁶ C. Romeike, M. R. Wegewijs, and H. Schoeller, Phys. Rev. Lett. **96**, 196805 (2006).
- ¹⁷ G. Gonzalez, M. N. Leuenberger, and E. R. Mucciolo, Phys. Rev. B **78**, 054445 (2008).
- ¹⁸ K. Park, E.-C. Yang, and D. N. Hendrickson, J. Appl. Phys. **97**, 10M522 (2005).
- ¹⁹ S. Barraza-Lopez, K. Park, V. Garcia-Suarez, and J. Ferrer, Phys. Rev. Lett. **102**, 246801 (2009).
- ²⁰ K. Park, S. Barraza-Lopez, V. M. Garcia-Suarez, and J. Ferrer, Phys. Rev. B **81**, 125447 (2010).
- ²¹ J. F. Nossa, M. F. Islam, C. M. Canali, and M. R. Pederson, Phys. Rev. B **85**, 085427 (2012).
- ²² F. Elste and C. Timm, Phys. Rev. B **71**, 155403 (2005).
- ²³ J. Lehmann and D. Loss, Phys. Rev. Lett. **98**, 117203 (2007).
- ²⁴ S. Herzog and M. R. Wegewijs, Nanotechnology **21**, 274010 (2010).
- ²⁵ F. Reckermann, M. Leijnse, and M. R. Wegewijs, Phys. Rev. B **79**, 075313 (2009).
- ²⁶ C. Romeike, M. R. Wegewijs, M. Ruben, W. Wenzel, and H. Schoeller, Phys. Rev. B. **75**, 064404 (2007).
- ²⁷ J. von Delft and C. L. Henley, Phys. Rev. Lett. **69**, 3226 (1992); A. Garg, Europhys. Lett. **22**, 205 (1993).
- ²⁸ M. Imada, A. Fujimori, and Y. Tokura, Rev. Mod. Phys. **70**, 1039 (1998).
- ²⁹ B. H. Kim and B. I. Min, New J. Phys. **13**, 073034 (2011).
- ³⁰ V. Yu. Yushankhai and R. Hayn, Europhys. Lett. **47**, 116 (1999).
- ³¹ I. A. Nekrasov, M. A. Korotin, and V. I. Anisimov, preprint, arXiv:cond-mat/0009107.
- ³² A. Bose and R. Chatterjee, Proc. Phys. Soc. **82**, 23 (1963).
- ³³ Z.-H. Zhang *et al.*, Mod. Phys. Lett. B **23**, 1415 (2009).
- ³⁴ F. Wang *et al.*, J. Magn. Magn. Mat. **329**, 88 (2013).
- ³⁵ R. Basler *et al.*, Inorg. Chem. **44**, 649 (2005).
- ³⁶ W. L. Feng *et al.*, J. Magn. Magn. Mater. **323**, 528 (2011).
- ³⁷ A. S. Zyazin *et al.*, Nanolett. **10**, 3307 (2010).
- ³⁸ C. W. J. Beenakker, Phys. Rev. B **44**, 1646 (1991).
- ³⁹ M. Urdampilleta, S. Klyatskaya, J.-P. Cleuziou, M. Ruben, and W. Wernsdorfer, Nature Mat. **10**, 502 (2011).
- ⁴⁰ E. Burzuri, A. S. Zyazin, A. Cornia, and H. S. J. van der Zant, Phys. Rev. Lett. **109**, 147203 (2012).
- ⁴¹ M. A. Aldamen *et al.*, J. Am. Chem. Soc. **130**, 8874 (2008).
- ⁴² M. A. Aldamen *et al.*, Inorg. Chem. **48**, 3467(2009).
- ⁴³ J. Titel *et al.*, J. Am. Chem. Soc. **133**, 15814 (2011).
- ⁴⁴ M. Martinez-Perez *et al.*, Phys. Rev. Lett. **108**, 247213 (2012).